

Fault detection from guided waves and tunnel surface waves of in-mine seismic data

Original

Fault detection from guided waves and tunnel surface waves of in-mine seismic data / KHOSRO ANJOM, Farbod; Colombero, Chiara; Socco, Laura. - (2022). (Intervento presentato al convegno 17th Biennial Conference & Exhibition).

Availability:

This version is available at: 11583/2973760 since: 2022-12-12T08:58:49Z

Publisher:

South African Geophysical Association (SAGA)

Published

DOI:

Terms of use:

This article is made available under terms and conditions as specified in the corresponding bibliographic description in the repository

Publisher copyright

(Article begins on next page)

Fault detection from guided waves and tunnel surface waves of in-mine seismic data

F. Khosro Anjom¹, C. Colombero¹, L.V. Socco¹

1. Politecnico di Torino, Italy, Khosro-anjom.farbod@polito.it

BIOGRAPHY

Farbod Khosro Anjom is post-doctoral fellow at Politecnico di Torino. His focus is on studying surface wave propagation and processing them to build the near-surface elastic parameters.

Chiara Colombero is assistant professor at Politecnico di Torino. Part of her research focuses on the exploitation of surface wave attributes for the identification of sharp lateral variations in the subsurface, with promising applications to mineral exploration.

Laura Valentina Socco is Full Professor of Geophysics at Politecnico di Torino. She works on seismic surface wave analysis and geophysical data integration. She received the Conrad Schlumberger Award (EAGE) in 2014 and the Outstanding Educator award (SEG) in 2019.

SUMMARY

With the increase in demand for mineral resources and depletion of conventional mines, the mineral exploration is moving to deeper targets, carrying more exploitation challenges and geological complexities. The imaging of structural discontinuities, such as faults and dykes, is also important to mitigate geo hazards. Here, we apply a method developed in the context of on-surface seismic for structural discontinuity detection on a synthetic in-mine seismic data set. 3D seismic wave propagation is simulated along a mine tunnel with simple, but realistic, geometry and geological background. The processing method involves the computation and interpretation of four attributes related to the propagation of the surface waves and guided waves that are sensitive to abrupt changes in the mechanical properties of the subsurface. Our test shows that these attributes are fast and effective in the detection of faults from the tunnel surface wave and guided waves, without the need for distinction of filtering of any seismic phase. Also, the comparison between the attributes of tunnel floor and ceiling arrays can provide useful information about the dipping of the faults.

INTRODUCTION

Constant mineral excavation has led to an increase in the depth of the mineral resources with rich ore grade. Mineral explorations from deep mines are usually associated with significant growth in cost and energy

consumption, as well as increase in geological complexities, such as faults and dykes (Eales and Cawthorn, 1996). Detection and location of these discontinuities is of utmost importance for mining plans and to prevent geohazards that may result in production halt and fatalities.

Seismic data from in-mine acquisitions have already proven to carry important information about the media surrounding the mine tunnels and can be used for the recognition of faults and other structural discontinuities (Rapetsoa et al., 2022).

In presence of a free surface, seismic surface waves are generated. These highly energetic waves travel parallel to the free surface and their amplitude decays exponentially with distance from the free surface. As a result, they attenuate less than the body waves and are usually the dominant event in the recordings. For these reasons, in on-surface surveys they play a key role for the reconstruction of lateral anomalies and structural discontinuities (e.g., Boiero and Socco, 2011).

Colombero et al. (2019) developed a fast and fully data-driven workflow for near-surface detection and location of geological variations, analysing the propagation of seismic surface waves through four attributes (i.e., energy, energy decay exponent, attenuation coefficient, and autospectrum). The method demonstrated effective in various synthetic and real data sets with different levels of complexity. Papadopoulou et al. (2021) showed that these attributes can be implemented in an automatic screening tool for fast and efficient site characterization in near real time.

These features make the method potentially useful and attractive for in-mine prospecting and operations. However, the propagation of seismic waves in the vicinity of mine tunnels is much more complex than in on-surface surveys. All the tunnel walls act as free surfaces and surface waves are expected to be generated along the tunnel direction. Moreover, the drilling of the tunnel significantly alters the equilibrium of forces close to the hole and creates the so-called excavation damage zone (EDZ). The EDZ usually affects a very thin portion of the tunnel walls (less than 1 m in depth) in which a reduction in the elastic properties is expected due to the cracks and fractures induced by the excavation. Consequently, seismic data from in-mine surveys include guided waves propagating within the EDZ and surface tunnel waves, which can superimpose and create complex propagation patterns that cannot be handled with traditional surface wave dispersion analyses.

Here, we aim at testing the surface wave attributes of Colombero et al. (2019) for detection and location of structural discontinuities on in-mine guided and tunnel surface seismic data, without discriminating them. We apply the method to a synthetic data set to verify the possibility of fast fault identification and dipping estimation directly from the raw data.

METHOD

We consider four surface wave attributes, highly sensitive to lateral variations, as implemented in Colombero et al. (2019) for multifold data. In summary:

- **Energy** (Nasseri Moghaddam et al., 2005) is the sum of the squared amplitudes of the seismic traces after geometrical spreading correction. Energy peaks are expected for the seismic traces recorded on low-velocity anomalies, such as faults and shear zones, as a result of the energy trapping and back reflections at the discontinuities edges.
- **Autospectrum or autospectral density** (Zerwer et al., 2005) is the sum of the squared real and imaginary values of the Fourier transform at each frequency. Consequently, it displays the distribution of the energy content at different frequencies/wavelengths, supporting the previous attribute interpretation and also providing a rough indication on the depth of the detected anomalies.
- **Energy decay exponent γ** (Bergamo and Socco, 2014) is the exponents that relates the offset and energy ratios of two subsequent recordings as:

$$\frac{E_{i+1}}{E_i} = \left(\frac{r_{i+1}}{r_i}\right)^{-\gamma}, \quad (1)$$

where E_i and r_i are the energy attribute and the distance from the source for the i th trace. Strong deviation of γ from zero indicates energy decay or concentration caused by the lateral heterogeneity. The energy decay exponent is computed for trace windows having both positive and negative offsets. In presence of lateral discontinuities, they are expected to show marked opposite oscillations at the lateral interface linked to the direction of wave propagation. In particular, energy concentrations can be observed passing from high-velocity to low-velocity materials, whereas energy decays are expected going through the opposite material contrast.

- **Attenuation coefficient α_f** (Bergamo and Socco, 2014) shows the attenuation of seismic wave at each frequency f and can be computed from the decomposed energy attributes of the two subsequent traces as:

$$E_{f,i+1} = E_{f,i} e^{-2\alpha_f(r_{i+1}-r_i)}. \quad (2)$$

Stacking the results (in absolute value) for positive and negative offsets, a clear delineation of the lateral discontinuity position can be obtained.

SYNTHETIC MODEL AND NUMERICAL SIMULATION

We created a 3D synthetic model based on the physical and elastic properties of a hypothetical deep mine. The

model is $1000 \text{ m} \times 500 \text{ m} \times 500 \text{ m}$ in x , y and depth directions, respectively. The tunnel is an $8 \text{ m} \times 8 \text{ m}$ rectangular horizontal tunnel in the centre of the model. The model includes 1 m of EDZ around the tunnel and a 5-m thick dipping fault (45° from the horizontal plane) crossing the tunnel. The properties of the background homogenous environment, EDZ and fault are provided in Table 1.

	VS (m/s)	VP (m/s)	Density (kg/m ³)
Background	2700	4450	2800
EDZ	2360	3850	2600
Fault	750	1500	2200

Table 1: The elastic parameters of the synthetic model. The properties of the tunnel are selected equal of air.

In Figure 1a, we show the vertical section of the S-wave velocity model along the tunnel at $y = 250 \text{ m}$. In Figure 2, we show a zoomed view (for better visualization of EDZ) of a horizontal section for S-wave velocity at depth 250 m.

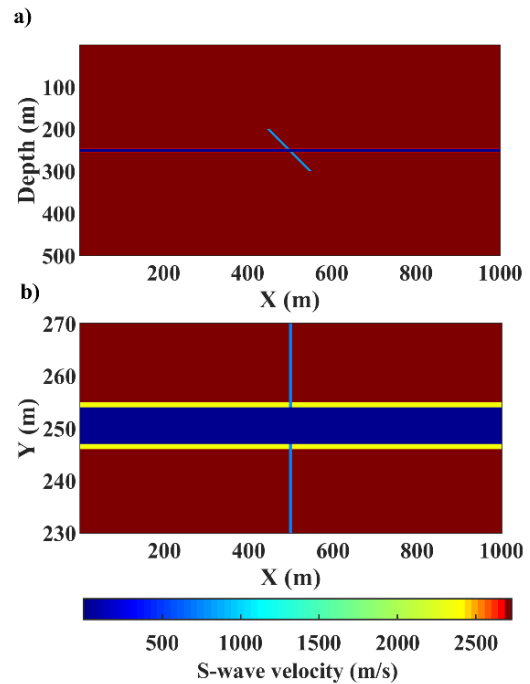


Figure 1. Slices of the S-wave velocity of the 3D synthetic model. (a) x-depth plane at $y = 250 \text{ m}$. (b) x-y plane at depth = 250 m. The yellow layers represent the EDZ.

We use SOFI3D, an open-source viscoelastic finite-difference algorithm (Bohlen, 2002), to simulate the 3D wave propagation in the model. The method discretises the wave equation using second-order spatial and temporal finite differences over a staggered grid (Virieux, 1986). The free surface condition along the tunnel is satisfied by imposing the properties of air to the tunnel volume and without explicitly defining free surface conditions across the boundaries of the tunnel (Bohlen and Saenger, 2006). No additional free surfaces

are imposed, and the model boundaries are simulated as absorbing boundaries to avoid back reflections from the model edges.

We use grid size of 1 m in each direction, that is small enough to mitigate numerical dispersion. The time step for the finite difference computation is selected as 0.1 ms to honour the Courant-Friedrich-Lewy criterion and maintain stability. We imposed constant quality factors (Q_p and Q_s) equal to 1000, considering spatially invariant intrinsic attenuation.

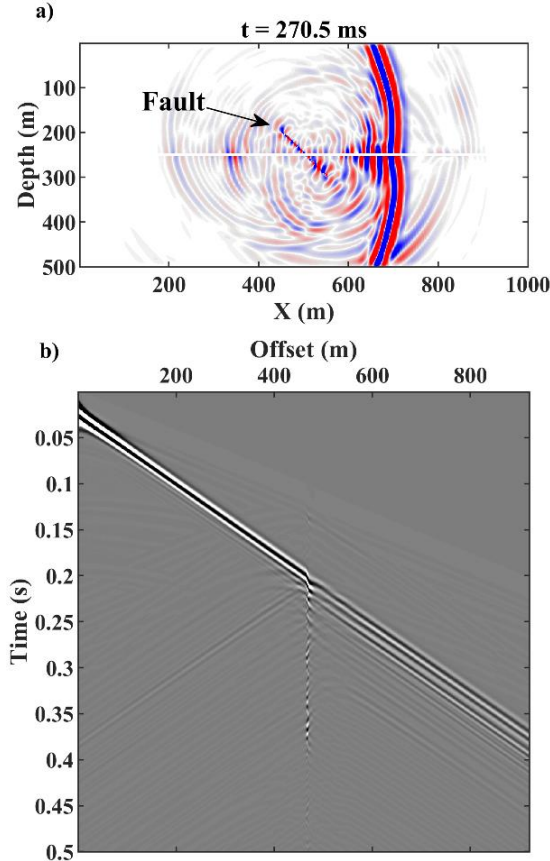


Figure 2. (a) Snapshot of the wave propagation on the x-depth plane at $y=250$ m and time equal to 270.5 ms. (b) Vertical component of the recorded data on the tunnel floor array. Both plots are from the shot located at $X=40$ m.

We simulate a seismic experiment with a line of receivers on the floor and one on the ceiling of the tunnel and a set of shot points on the tunnel floor. We define four locations ($X=40$ m, 347 m, 654 m and 961 m) on the floor of the tunnel to impose vertical point source (65-Hz Ricker wavelet). The three displacement velocity components are recorded at 920 receiver locations on the floor and 920 receiver locations on the ceiling. The receiver arrays start at $X=41$ m up to $X=960$ m with 1 m inter-receiver spacing. Here, we only consider the vertical component to compute the attributes. The data are recorded with 0.5 ms sampling interval for a duration of 0.5 s. In Figure 2a, we show a snapshot of the vertical displacement velocity after 270.5 ms from shooting. A significant amount of energy is trapped within the fault area. In Figure 2b, we show the vertical component of the data recorded by the receivers from the same shot

location as Figure 1b ($X=40$ m). The data are significantly attenuated after passing through the fault (~offset 460 m).

RESULTS

In Figure 3, we show the estimated attributes on the tunnel floor and ceiling arrays, zoomed on the centre of the line ($X=400$ m–600 m), close to the fault location.

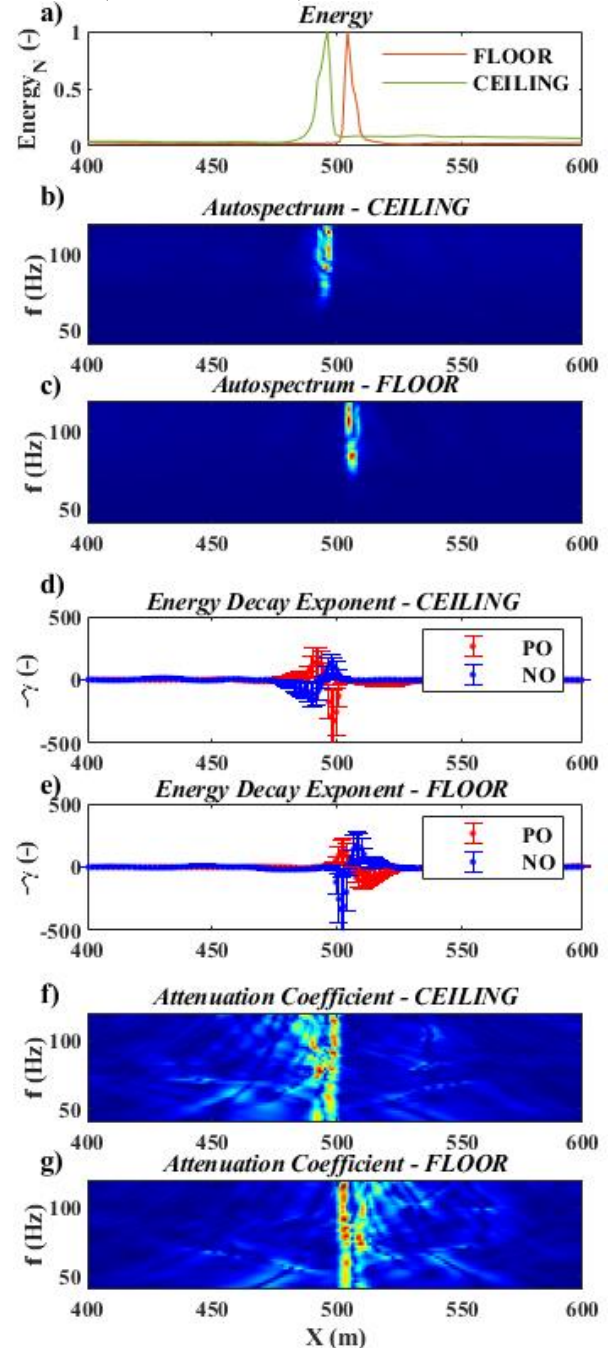


Figure 3. The estimated attributes for the synthetic data set between positions 400 m and 600 m using the floor and ceiling receiver arrays. (a) Energy attributes of floor and ceiling array. (b) and (c) Autospectrum of the ceiling and floor arrays. (d) and (e) Energy decay exponent of the ceiling and floor arrays. (f) and (g) Attenuation coefficient of the ceiling and floor arrays.

The estimated energy attribute for the floor and the ceiling are shown in Figure 3a, whereas the autospectrum attribute, energy decay coefficient and attenuation attributes are plotted separately for the floor and ceiling arrays (Figures 3b to g). All attributes, show high amplitude in the proximity of the fault location and values close to zero elsewhere. The energy attribute provides a sharp increase at the fault location along each array, as expected for anomalies having lower velocity than surrounding materials (Figure 3a). The autospectrum coherently shows two high energy spikes within the fault zone for frequencies higher than 65 Hz (Figures 3b and c). Similarly, the energy decay exponents (Figures 3d and e) show significant changes in $-\gamma$ value. We plot the values of $-\gamma$ such that the maxima correspond to energy concentrations and the minima correspond to energy decays. Positive and negative offset curves correspond to spatial windows located at the right and left sides respectively of each shot positions. Along both arrays, energy concentrations can be observed passing from the intact rock to the fault zone, whereas energy decays are depicted in the opposite direction. The stacked attenuation coefficients (Figures 3f and 3g) suggest strong attenuation within a significant frequency range. The frequency band affected by the anomaly is maximum at the location of the fault crossing the array, while it decreases on opposite sides for the floor and ceiling arrays. Comparing the floor and ceiling attributes, there is a slight but systematic shift in the position of the attribute anomalies. This shift is linked to the dip of the fault and to the fact that it intersects the tunnel at different locations on the floor and ceiling (Figure 1a and points A and B in Figure 4).

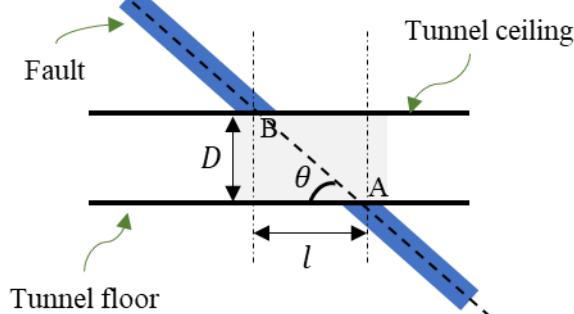


Figure 4. Schematic view of a dipping fault crossing the mining tunnel. An illustration why the attributes from the floor and ceiling receiver arrays depict the faults at different location.

We use the shift in the attribute plots and the height of the tunnel (l and D in Figure 4) to estimate the fault dip. Since the shift between the floor and ceiling attributes is sharper and easy to identify in the energy plot (Figure 3a), we pick the position of the energy attribute maxima, which are at positions 496 m (ceiling, B in Figure 4) and 504 m (floor, A in Figure 4). Then, we use the distance of 8 m between the peaks to estimate the fault dip as:

$$\theta = \tan^{-1}\left(\frac{D}{l}\right). \quad (3)$$

Given that the height of the tunnel is 8 m, a θ (Figure 4) of 45° is obtained from equation 3, which exactly matches the true angle of the simulated fault.

CONCLUSIONS

Surface wave attributes have been proven to be very useful in detecting and locating lateral anomalies in on-surface seismic surveys. Here, we showed that the same attributes can be applied to in-mine seismic data not only to quickly identify the presence of faults crossing the tunnel but also to potentially predict their dip. The attributes can be applied directly to raw data and show good potential for fast and reliable screening of the tunnel walls. Nevertheless, more synthetic tests with different noise levels and real tests will be performed to evaluate the efficiency of the method in complex structural and geological environments. In future works, we also aim at analysing, discriminating, and inverting the dispersion curves of the tunnel surface wave and guided wave to obtain the S-wave and P-wave velocity models in the proximity of the tunnel, for a comprehensive characterization of the materials in support to mining exploration.

ACKNOWLEDGMENTS

This research is funded by FUTURE project of ERA-NET Cofund on Raw Materials (ERA-MIN3). Computational resources were provided by hpc@polito, which is a project of Academic Computing within the Department of Control and Computer Engineering at the Politecnico di Torino.

REFERENCES

- Bergamo, P., and Socco, L.V., 2014, Detection of sharp later discontinuities through the analysis of surface-wave propagation: *Geophysics*, 79, 77–90
- Bohlen, T., 2002, Parallel 3-D viscoelastic finite difference seismic modelling: *Computers & Geosciences*, 28, 887–899.
- Bohlen, T. and Saenger E.H., 2006, Accuracy of heterogeneous staggered-grid finite-difference modeling of Rayleigh waves: *Geophysics*, 71, 109–115
- Boiero, D., and Socco, L.V., 2011, The meaning of surface wave dispersion curves in weakly laterally varying structures: *Near Surface Geophysics*, 9, 561–570
- Colombero, C., Comina, C., and Socco L.V., 2019, Imaging near-surface sharp lateral variations with surface-wave methods—Part 1: Detection and location, *Geophysics*, 84, 93–111
- Eales, H.V. and Cawthorn, R.G., 1996, The Bushveld complex: *Developments in Petrology*, 15, 181–229
- Nasseri-Moghaddam, A., Cascante, G., and Hutchinson, J., 2005, A new quantitative procedure to determine the location and embedment depth of a void using surface waves: *Journal of Environmental and Engineering Geophysics*, 10, 51–64.

- Papadopoulou, M., Colombero, C., Staring, M., Singer, J., Eddies, R., Flidner, M., Janod, F., and Socco, L.V., 2021, Fast near-surface investigation with surface-wave attributes: 2nd Conference on Geophysics for Infrastructure Planning, Monitoring and BIM, Held at Near Surface Geoscience Conference and Exhibition.
- Rapetsoa, M.K., Manzi, M.S.D., Westgate, M., Sihoyiya, M., James, I., Onyebueke, E., Kubeka, P., Durrheim, R.J., and Kgarume, T., 2022: Cost-effective in-mine seismic experiments to image platinum deposits and associated geological structures at Maseve platinum mine, South Africa, Near Surface Geophysics.
- Virieux, J., 1986, P-SV Wave Propagation in Heterogeneous Media: Velocity-Stress Finite-Difference Method: Geophysics, 51, 889-901.
- Zerwer, A., Polak, M.A., and Santamarina, J.C., 2005, Detection of surface breaking cracks in concrete members using Rayleigh waves: Journal of Environmental and Engineering Geophysics, 10, 295–306